Quarterly Progress Report

For Period

January 1 to March 31, 1967

FUNDAMENTAL STUDIES OF THE METALLURGICAL,
ELECTRICAL, AND OPTICAL PROPERTIES OF
GALLIUM PHOSPHIDE

Grant No. NsG-555—

Prepared For

NATIONAL AERONAUTICS AND SPACE ADMINISTRATION
LEWIS RESEARCH CENTER
CLEVELAND, OHIO

Work Performed By

Solid-State Electronics Laboratories
Stanford University
Stanford, California

PROJECT 5109: PHOTOELECTRICAL AND OPTICAL PROPERTIES OF GaP
CONTAINING TRIVALENT IRON AND COBALT IMPURITIES

National Aeronautics and Space Administration
Grant NsG 555
Project Leader: G. L. Pearson
Staff: J. Baranowski

In the last two quarters we reported the spectra of
divalent iron and cobalt in GaP, GaAs and several II-VI compounds.
We indicated that these spectra can be interpeted on the basis of
crystal field theory. In this quarter we investigated the photo-
electrical and optical properties of GaP with unfilled cobalt or iron
levels. The amount of iron and cobalt which was introduced into the
sample was much higher than the number of shallow donors present in the
sample, thus we have trivalent iron and cobalt in GaP.

1. Photoconductivity of GaP Containing Trivalent Co and Fe Impurities

Two of the samples were prepared from an n-type single
crystal of GaP in which $n = 5x10^{15}$ cm^{-3} and $\mu = 120$ cm^2/volt-sec at
room temperature. Cobalt was introduced by diffusion at 1300°C for
24 hours which gave an impurity concentration[1] of approximately 10^{18} cm^{-3}
in sample no. C2. Iron was introduced by diffusion under the same
conditions in sample no. F1.(We believe the impurity concentration in
this sample is also about 10^{18} cm^{-3}.) Sample no. C1 was prepared
from material supplied by D. H. Loescher and contained approximately
$1x10^{17}$ cm^{-3} cobalt impurity atoms. All samples were p-type after the
introduction of impurities. Contacts were applied at either end of
a rod-type sample by alloying thin evaporated layers of 98 gold-2 zinc
at 500°C in forming gas. Electrical tests indicated that the contacts

were ohmic, although a small photovoltaic effect appeared under illumination. Illumination was from a tungsten lamp and photocurrents were measured by a dc method. The measured photocurrents were corrected by subtracting out the part due to photovoltaic effect under zero applied voltage.

Measurements were made as a function of temperature under constant illumination and at a fixed bias. In all cases, the photocurrent, i_{pc} = total current - dark current - photovoltaic current, saturated at elevated temperatures but decreased with decreasing temperature and finally saturated again at low temperatures. The data for the two GaP:Co samples are shown in Fig. 1 and those for the single GaP:Fe sample in Fig. 2. In each case, $\ln i_{pc}$ is plotted versus $10^3/T$. Similar behavior was observed when the illumination was passed through a silicon filter thus eliminating all photons having energies greater than 1 eV. Since the band gap of GaP is 2.3 eV, this result indicates that only holes are responsible for the observed photoconductivity. The spectral distribution of photoresponse at room temperatures for sample no. C2 is presented in Fig. 3. This distribution is not corrected for variations in the number of photons which fall on the sample nor for variations in the number of photons which are absorbed.

We expect the Fermi level to be below the impurity acceptor level since our optical transmission measurements failed to show a d^7 configuration in GaP:Co or a d^6 configuration in GaP:Fe. Furthermore, we are certainly dealing with unfilled deep acceptor levels since Co and Fe impurity concentrations of 10^{17} to 10^{18} cm^{-3}

are much greater than the residual concentration of shallow donors in our GaP crystals. These data and arguments support the conclusion that the photocurrent is caused by the creation of free holes by exitation of electrons from different depths in the valence band to unfilled acceptor levels. The peaks of the photoresponse are probably connected with a higher absorption of photons thus producing a larger number of free holes. This problem will be discussed in section two.

ℓn dark currents (i_{dark} is proportional to resistivity) are plotted as a function of $10^3/T$ in Fig. 4 for all our samples. The slopes of the straight lines give the approximate position of the Fermi level. These slopes are greater than the straight line portions of the curves presented in Figs. 1 and 2. In order to explain our experimental results, we adopt the following model.

Under thermal equilibrium both ionized acceptor centers N_{ao}^- and non-ionized acceptor centers ($N_a - N_{ao}^-$) are present, where N_a is the number of cobalt or iron impurities. The number of ionized acceptors N_{ao}^- is approximately equal to the number of ionized shallow donors and is much smaller than the number of non-ionized acceptors. This implies that the Fermi level is slightly below the deep acceptor level. Electrons exited from the valence band by light are captured by acceptors in two ways. One is by transitions of electrons from different places in the valence band to acceptors with emission or absorption of phonons to conserve momentum. The other is by capture of electrons which were exited to the conduction band. We assume that the trivalent acceptors have a very high capture cross section for electrons, thus the lifetime of electrons in the conduction band

is very short. They are captured by the acceptors almost immediately and therefore the contribution from the presence of elctrons in the conduction band to the photocurrent is negligible. Acceptors which have captured one electron are divalent and can still capture another one, but the probability that they will capture a hole is very small. Therefore the electrons will stay at the acceptor levels for a long time. This leads to a long lifetime of electrons at the acceptor levels. We assume that the recombination of electrons from the acceptor levels with holes in the valence band is a direct process (there is no trapping process). Therefore the lifetime of free holes τ_p will be equal to the lifetime of electrons at acceptor levels. This lifetime will determine the photoconductivity behavior.

We first calculate the hole lifetime τ_p. Since the non-equilibrium recombination rate R' is proportional to the total number of free holes p and the total number of electrons captured by acceptor level N_a^- , we may write:

$$R' = A \, N_a^- \, p \quad ,$$

where

$$N_a^- = N_{ao}^- + \Delta N^-$$

$$N_{ao}^- = N_a \exp \left[- \frac{E_a - E_f}{kT} \right] = \text{the number of filled acceptors under thermal equilibrium}$$

N_a = the total number of cobalt or iron centers

ΔN^- = the number of electrons generated by light from the valence band and captured by acceptor levels

$p = p_o + \Delta p$

- 4 -

$$p_o = N_v \exp(-E_f/kT) = \text{the number of holes under thermal}$$
$$\text{equilibrium}$$

$$\Delta p = \text{the number of optically generated holes}$$

$$E_f \text{ and } E_a = \text{the energy of the Fermi level and the energy of}$$
$$\text{the unfilled acceptor levels respectively, both}$$
$$\text{measured from the top of the valence band}$$

We have $N_{ao}^- > p_o$ because of compensation of shallow donors by deep acceptors and we assume that $\Delta N^- = \Delta p$. The recombination rate R for thermal equilibrium is $R = A\, N_{ao}^-\, p_o$, so that $A = \dfrac{R}{N_{ao}^-\, p_o}$. In the case of weak illumination when $\Delta p < p_o$, from the definition of the hole lifetime τ_p ,

$$R' - R = \frac{\Delta p}{\tau_p} = \frac{R}{N_{ao}^-\, p_o}\ (N_a^-\, p - N_{ao}^-\, p_o)$$

$$= \frac{R}{N_{ao}^-\, p_o}\ (N_{ao}^-\, \Delta p + p_o\, \Delta N^- + \Delta N^-\, \Delta p)$$

$$= \frac{R}{N_{ao}^-\, p_o}\ \left[(N_{ao}^- + \Delta N^-) + p_o\right] \Delta p .$$

Because of the conditions $N_{ao}^- > p_o$ and $\Delta N^- < N_{ao}^-$

$$\frac{\Delta p}{\tau_p} \approx \frac{R\Delta p}{p_o} \quad ,$$

so that we have

$$\tau_p = \frac{N_v}{R} \exp\left(-\frac{E_f}{kT}\right)$$

and

$$\ln i_{pc} \sim \ln \tau_p \sim \ln \frac{N_v}{R} - \frac{E_f}{kT} .$$

It is difficult to estimate what the exact function of temperature gives the ratio of the density of states in the valence band N_v to the recombination rate R because R can be either radiative, non-radiative, or a combination of both. Assuming that transitions from acceptor levels to the valence band are radiative, we can calculate R following the method proposed by W. van Roosbroeck and W. Shockley.[2] The recombination rate under thermal equilibrium is equal to the generation rate for each interval of light frequency $d\nu$

$$R(\nu)\ d\nu = \frac{N(\nu)}{\tau(\nu)}\ d\nu\ ,$$

where

$\qquad N(\nu)$ = the number of photons of frequency ν as given by Plank's law

$\qquad \tau(\nu) = [\alpha(\nu)\ v_g]^{-1}$ = the "lifetime" of the photon equal to the product of an absorption coefficient α and the group velocity of the photon in the medium.

To obtain the total recombination rate R we have to integrate over all values of ν. In this way we obtain

$$R \sim T^3 \int_0^\infty \frac{\alpha(x)\,[n(x)]^2\,x^3\,dx}{\exp(x) - 1}\ ,$$

where

$\qquad x = \dfrac{h\nu}{kT}$

$\qquad \alpha(x)$ = absorption coefficient

$\qquad n(x)$ = refraction coefficient

so that we have

$$\frac{N_v}{R} \sim T^{-3/2} \left[\int_0^\infty \frac{\alpha(x)[n(x)]^2 x^3 \, dx}{\exp(x) - 1} \right]^{-1} .$$

The exact dependence of the ratio $\frac{N_v}{R}$ on temperature will depend on the right form of absorption coefficient $\alpha(x)$ connected with transitions from the valence band to acceptor levels and how $\alpha(x)$ depends on temperature. The above integral is appreciable only over a narrow range of frequencies because of the rapid increase in $\exp(x)$ as ν increases, and because of a decrease in $\alpha(x)$ for values of ν smaller than that corresponding to transitions from the top of the valence band to the acceptor levels. The above calculations neglect the contribution from non-radiative recombination which if present, can change the above temperature dependence.

At the present time we can only say that the ratio $\frac{N_v}{R}$ will increase with decreasing temperature giving the slope of the plot of $\ln i_{pc}$ versus $\frac{10^3}{T}$ which is smaller than E_f. This is in agreement with our data. Summarizing, the model which we have presented here can qualitatively explain the decrease of photcurrent with decreasing temperature without assuming the existance of other levels than those of the impurity acceptor centers. At low temperature the concentration of thermally generated holes is very small so that under sufficient illumination $\Delta p > p_0$. In this case, (as is the case at strong illumination) τ_p and therefore i_{pc} should not change drastically with temperature. This behavior was observed in GaP:Co since all the curves in Fig. 1 become flat at low temperatures. Further verification of the analysis is seen in this figure where we plot

ℓn i_{pc} for sample no. C1 at two different light intensities. Reducing the illumination by a factor of 10 shifts the threshold of saturation to a lower temperature. The low temperature saturation range in the sample with iron is apparently below the lower limit of our present measuring equipment. From the slopes of ℓn i_{dark} and ℓn i_{pc} for the sample with iron we can estimate that the acceptor level is around 0.1 eV above the top of the valence band. The reason for saturation of i_{pc} at high temperatures is not obvious. A possible explanation is that the assumption $N_{ao}^{-} > p_o$ no longer holds. In this case the lifetime τ_p will be given by an expression:

$$\frac{1}{\tau_p} = \frac{R}{N_v} \exp \frac{E_f}{kT} + \frac{R}{N_a} \exp \frac{E_a - E_f}{kT}$$

Because $\frac{R}{N_a} > \frac{R}{N_v}$, with increasing temperature, the second term will exceed the first one at some value of T. In this case, because E_a and E_f are very close to each other the increase of R with temperature can be compensated by a decrease of the term $\exp \frac{E_a - E_f}{kT}$ and the lifetime will be a weak function of temperature or even independent of temperature.

A decrease of photocurrent with decreasing temperature has been observed in GaAs: Cu [3] and ZnS: Cu [4]. In both cases the explanation was based on the assumption of the existance of additional electron traps close to the conduction band. Our data indicate that only holes are responsible for photoconductivity and that electrons exited from the valence band are captured by unfilled acceptors levels. It is interesting to note that this type of behavior of photoconductivity was observed only when the Fermi level was below acceptor levels formed

by transition metal impurities. This evidence supports our
explanation of this penomenon. The model proposed here allows us
to predict that we could expect a decrease of photocurrent with
decreasing temperature at some temperature range in all III-V compounds
doped with transition metals (only if such impurities produced deep acceptor
levels) and in all II-VI compounds doped with chromium or copper. The
Fermi level must of course be below the acceptor level. In all of
these cases we can expect photoconductivity to be connected with the
creation of free holes and the capture of electrons in bonding orbitals
of acceptor complexes.

2. Optical Properties of GaP Containing Trivalent Co.

The absorption measurements on single crystals of GaP
doped with cobalt are reported here. The cobalt was diffused under
the same conditions as for sample no. C2. The transmission curves
at three different temperatures are shown in Fig. 5. We saw no trace
of a d^7 configuration so we can conclude that we have trivalent cobalt
centers in the lattice. Three electrons are needed for the bonding
(cobalt substitutes for gallium). Since the number of cobalt centers
exceeds the number of shallow donors, we can expect that one of the
d-electrons will be taken to the bonding orbitals, thus leaving a
d^6 configuration. Transmission curves taken at liquid helium did not
show a characteristic spectrum of the d^6 configuration. This indicates
that the d-electrons in bonding orbitals distort the d-shell of elec-
trons and that the crystal field model is inapplicable to such complexes.
There is a broad absorption ranging from 3.3 μ to the absorption
edge. This can be caused by transitions from different positions in

the valence band in k-space to the acceptor levels. The increase of absorption with increase in light energy can reflect the increase in density of states when we are going deep into the valence band. The peak at 1.06 μ may be caused by a transition from the L point at the edge of the Brillouin zone where the density of states has a peak. Because the cobalt level is 0.4 ev above the top of the valence band, this assignment indicates that the valence band at the L point is 0.77 ev below the top of the valence band at the Γ point. This is not bad agreement with calculations by M. L. Cohen and T. K. Bergstrasser[5] who give a 0.9 eV value. There is one other peak on the broad absorption around 0.7 μ. These two peaks appear also in a spectral distribution of photoconductivity (see Fig. 3). At the present time we do not have a good explanation for the appearance of the 0.7 μ peak. We are going to investigate this problem during the next quarter.

REFERENCES

1. D. H. Loescher, Technical Report No. 5109-2, Stanford Electronics Laboratories, Stanford, California, October 1966.

2. W. van Roosbroeck, W. Shockley, Phys. Rev., 94, 1558 (1954).

3. J. Blanc, R. H. Bube, and H. E. MacDonald, Jour. Appl. Phys., 32, 1666 (1961).

4. G. Blount, Stanford Ph.D. thesis.
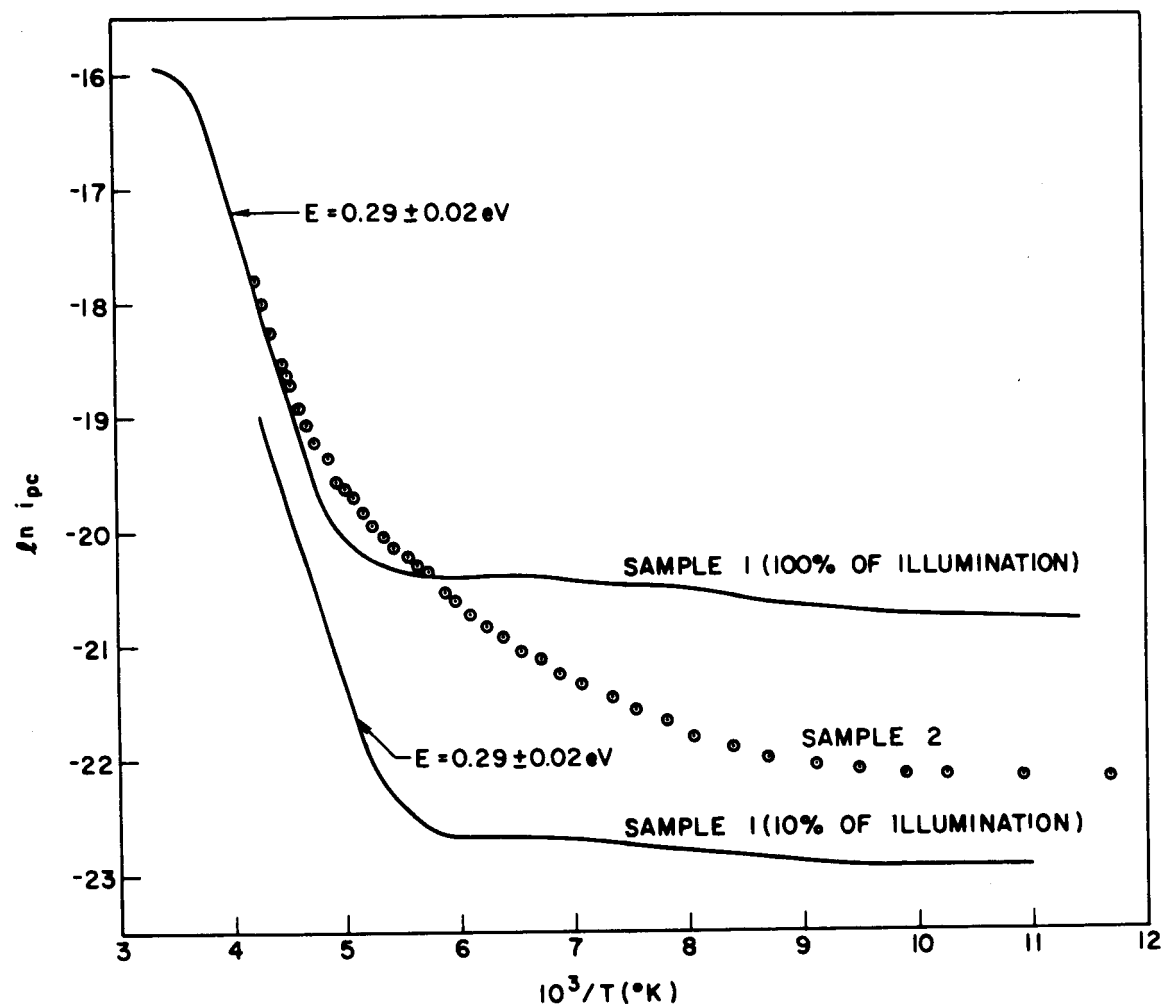
5. M. L. Cohen, T. K. Bergstresser, Phys. Rev., 141, 789 (1966).

Fig. 1

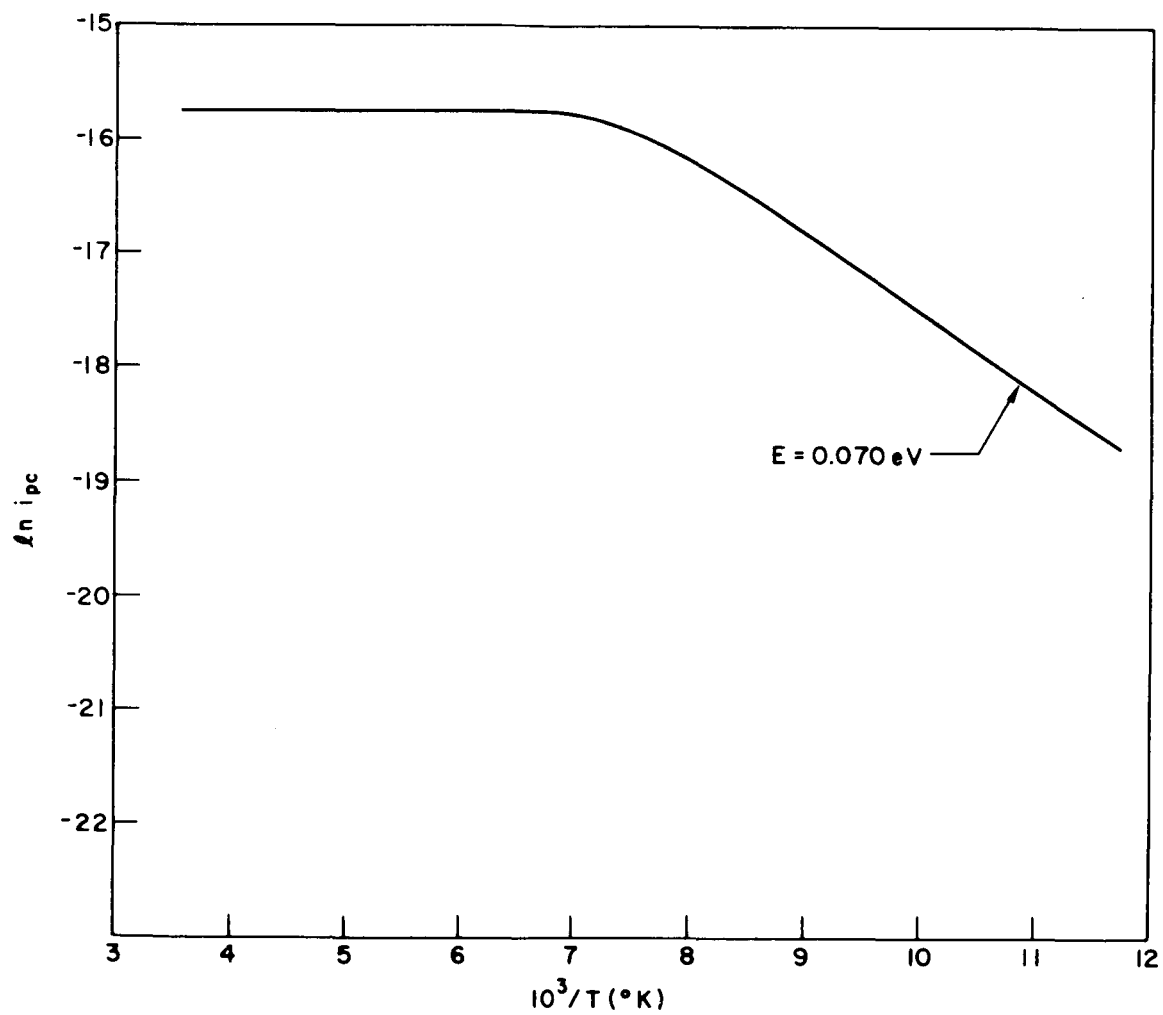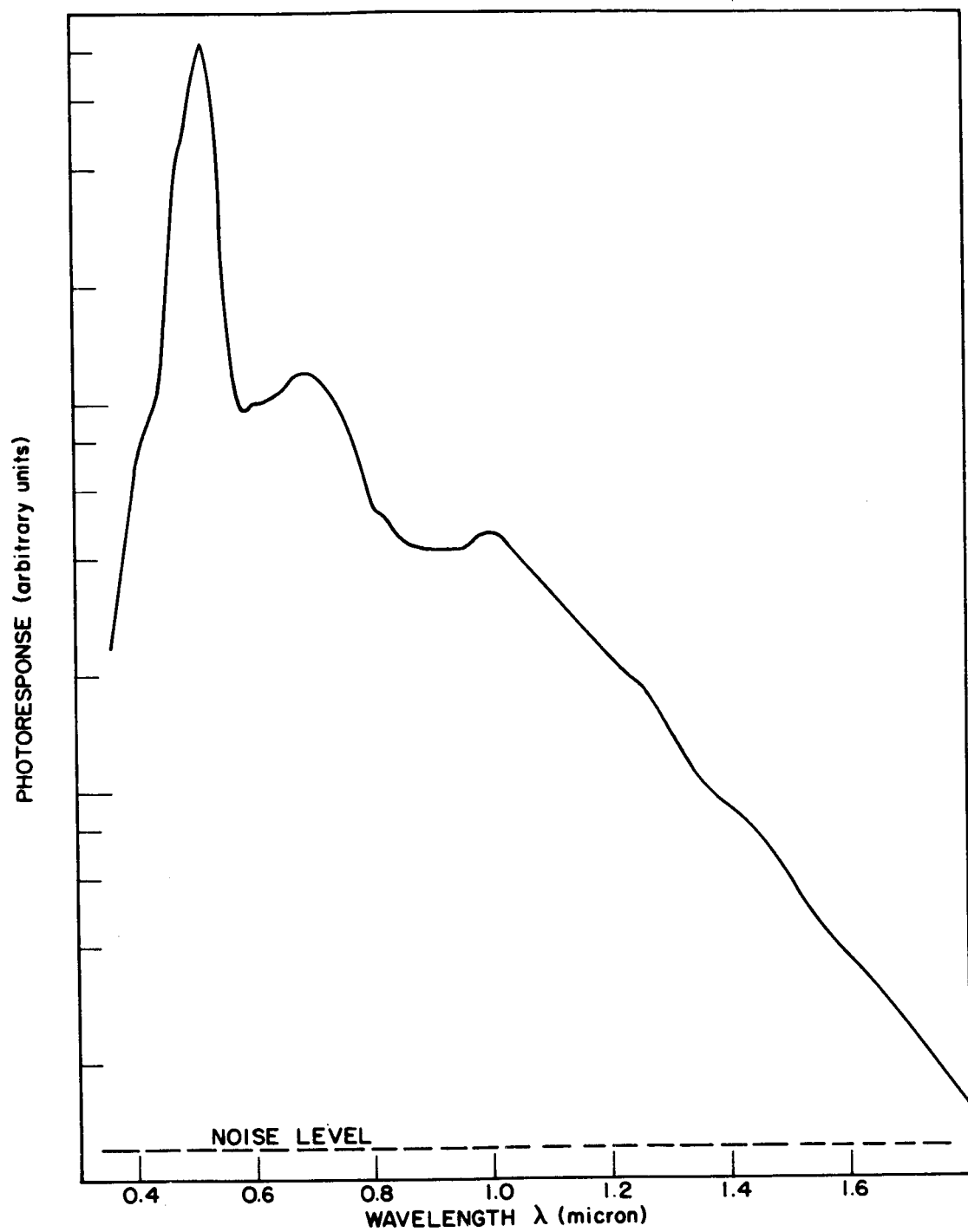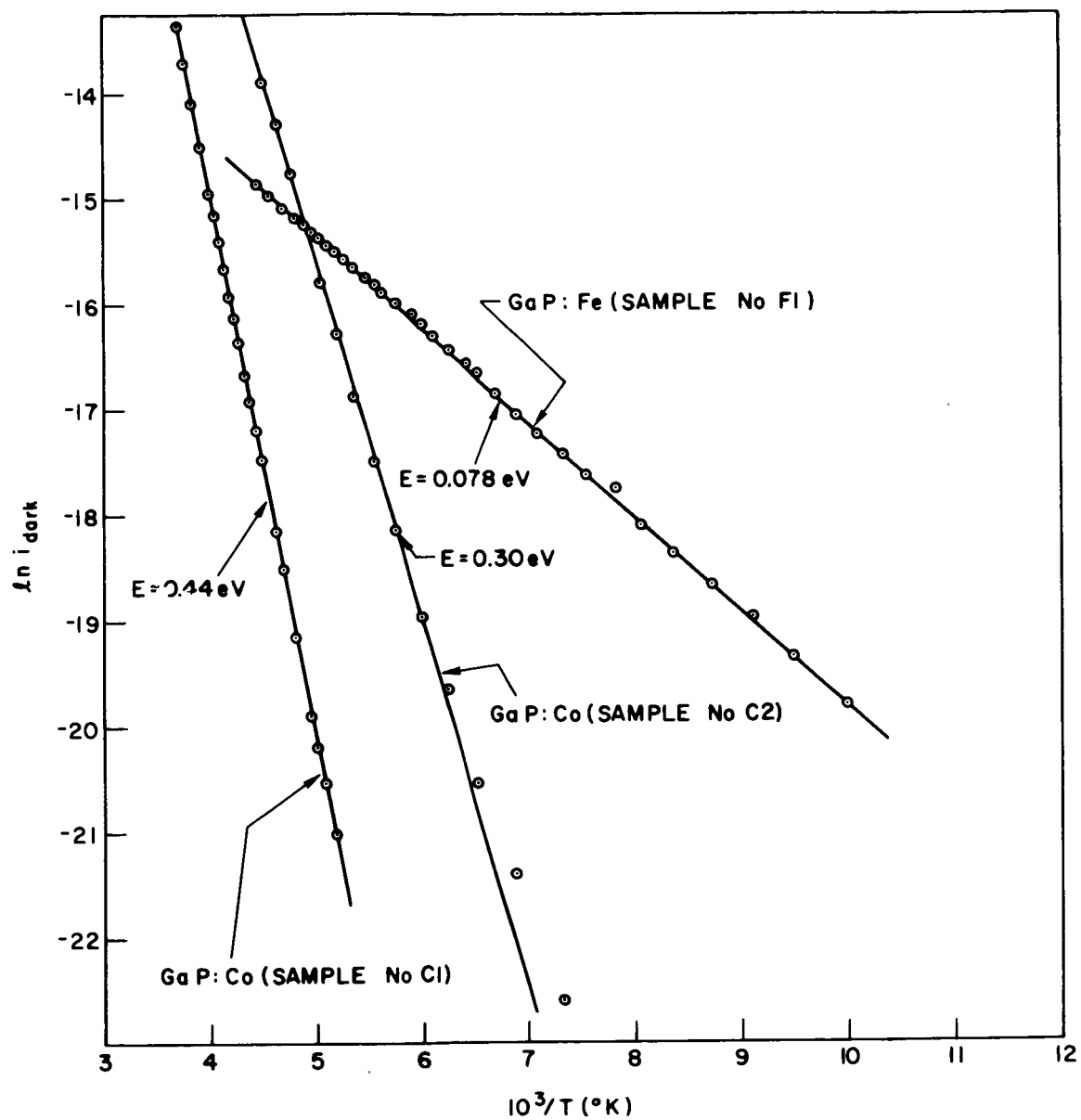Fig. 2

Fig. 3

Fig. 4
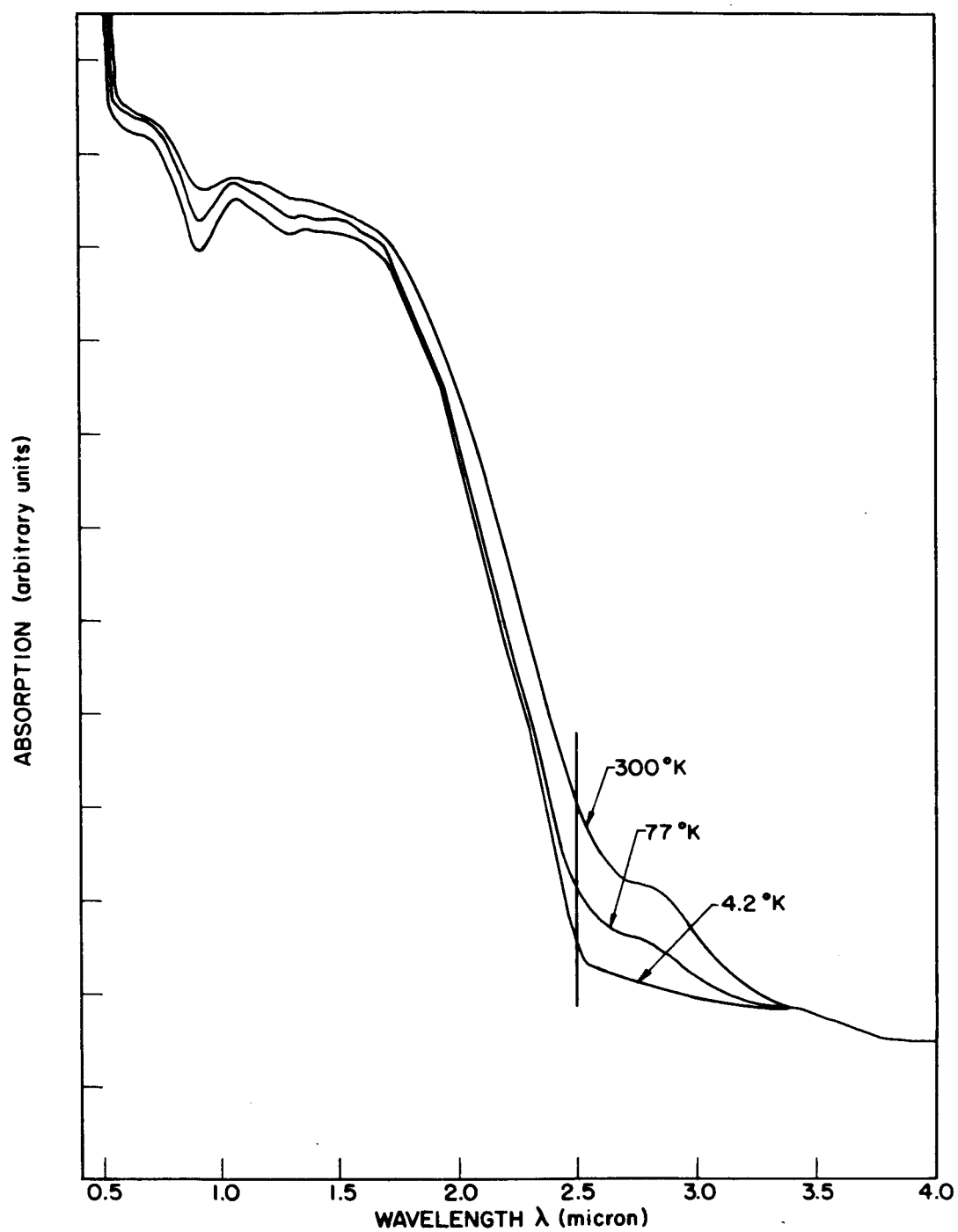
Fig. 5

PROJECT 5112:   THE PROPERTIES OF RECTIFYING JUNCTIONS IN $GaAs_x P_{1-x}$

National Aeronautics and Space Administration
Grant NsG-555
Project Leader: G. L. Pearson
Staff: S. F. Nygren*

The purpose of this project is to study the preparation

and characterization of rectifying junctions in GaP and $GaAs_x P_{1-x}$.

In particular, we wish to relate the structure of the crystals to

the electrical properties of the junctions. This quarter we have

finished most of our study of imperfections in vapor grown GaP. We

have concluded that the dominant imperfections are dislocations and

stacking faults. We have also made preliminary observations of the

diffusion of zinc into GaP. We have found that both types of

imperfections appear to act as diffusion short circuits.

<div align="center">Identification of Defects</div>

A. Experimental

Imperfections in undoped GaP crystals may be revealed

by etching various crystallographic planes of the crystals in

suitable solutions. When a {110} cleavage face is etched in 9 HNO_3:

1 HF: 5 H_2O for a few minutes, the pattern shown in Fig. 1 develops.

The irregular lines and steps running from the substrate to the growth

surface may be disregarded since they are simply steps that indicate

imperfect cleavage. The important feature is the set of lines that

runs parallel to the growth surface of the crystal. These lines are

often seen in GaP that is grown by vapor epitaxy in this laboratory.

The opposite {111} faces of GaP are different from each other and must be etched differently. Both faces must be mechanically polished in 0.3 μ grit before etching to insure a reliable etch pattern. The {111}Ga face may then be etched for 10 minutes at room temperature in a solution of 8g $K_3Fe (CN)_6$:12g KOH:100g H_2O. Typical results are shown in Fig. 2. The etch pattern consists mainly of lines and approximately triangular pits. We have shown in a previous report[1] that the lines are traces of {111} planes. Thus, they must always meet at 60° on 120° angles.

We note that the crystal may be completely oriented from either the etch pits or lines since the pits are triangular and the lines are formed by grooves that have one wall steeper than the other. The crystal orientation is shown schematically in Fig. 3. This orientation is confirmed by using it to find one of the {111} planes that is inclined to the surface. This orientation of etch pits is in contrast to the orientation of etch pits in silicon. Booker and Stickler[2] find that etch pits in silicon form triangles whose vertices always point in $<\bar{2}11>$ directions. We find that etch pit triangles in GaP always point in $<2\bar{1}\bar{1}>$ directions.

The {111}P face of GaP may be etched in hot aqua regia. Generally an etch pattern will appear after about 2 minutes, but continued etching will often erase the pattern again. Hot aqua regia also etches the {111}Ga face of GaP, so when a pattern is developed on {111}P, a course but usable pattern will also be present on {111}Ga. Figure 4a shows the etch pattern on the {111}P face of a typical GaP crystal, and Fig. 4b shows the pattern on the {111}Ga

face of the same crystal. The two pictures may be compared directly since the photomicrograph of Fig. 4b was taken by simply refocusing the microscope after taking the photomicrograph of Fig. 4a. We see that while both pits and lines appear on the {111}Ga face, only lines appear on the {111}P face. Also, the lines on the {111}Ga face correspond exactly to the lines on the {111}P face. All apparent discrepancies can be accounted for by noting that the crystal is 75 μ thick and that the imperfections could easily interact and change slightly in that thickness.

To further study defects in vapor grown GaP, a crystal was oriented according to the etch pattern and then was cross sectioned to reveal a {111}Ga plane that was inclined to the surface of the crystal. The GaAs substrate was removed from the GaP by etching so that very little of the GaP would be removed. Then the {111}Ga growth surface and the {111}Ga cross section were polished and etched in the {111}Ga solution. The resulting etch pattern is shown in Fig. 5. Several features of this pattern are significant. First, this is the same crystal as is shown in Fig. 1. We see that the lines that appeared on the {110} face do not appear on the {111}Ga cross section. Hence, the defect that is shown in Fig. 1 is neither a set of dislocations (which would have been revealed as etch pits on {111}Ga) nor are they the kind of defect that gives lines on {111}Ga. MacKenna[3] shows similar etch patterns in silicon and attributes them to impurity segregation. We might have the same effect here.

Another important feature is the interaction of the lines. They often intersect, and then only one will proceed onward.

- 3 -

Lastly, we note a very high concentration of etch pits in the region of the crystal that was closest to the substrate. In other work we have noticed that the region of the GaP overgrowth close to the periphery of the seed is also highly defective. Hence, if GaP grown by vapor epitaxy is to be used for electrical measurements or for fabrication of devices, the 75 μ closest to the substrate and the 1-2 mm closest to the edge of the overgrowth should be discarded.

To make a more careful study of the interactions among the crystal defects that lead to lines in the etch patterns, a GaP crystal was polished, etched, and photographed. Next it was lapped until it was 25-50 μ thinner. Then it was polished, lapped and photographed again. This sequence was continued until four pictures had been taken. The interactions among etch lines that were observed are shown schematically in Fig. 6. We see that the lines may get either longer or shorter as the crystal grows thicker.

We also tried to use Berg-Barrett x-ray topography to help identify the crystal defects. In this technique, the crystal is oriented so that an incident x-ray beam strikes the crystal at the Bragg angle. The beam is then reflected from the surface of the crystal and used to expose a photographic plate. We used a scanning topographic camera manufactured by Crystallogenics Incorporated. It is designed so that the crystal moves back and forth under the x-ray beam in such a way that an image of the entire crystal is mapped onto the photographic plate. Figure 7 shows a typical result. The radiation was Cu Kα_1 at 36 Kv and 4 ma; the film was Ilford Nuclear Research Plate, type L-4, 50 μ emulsion; exposure time was 1.5 hours.

- 4 -

If the crystal were perfect, the film would be uniformly exposed. Any lighter shadings, then, represent crystal defects that are within a few microns of the surface (since the x-ray penetration is only that deep). The fact that only part of the crystal is in contrast indicates that the crystal is slightly warped so that the Bragg reflection criterion cannot be met for the entire crystal at once. The white spot slightly above the center of the crystal is a gross imperfection, possibly a polycrystalline inclusion. The curved white lines running in random directions are scratch marks. The white lines running in < 110 > directions represent defects that are parallel to {111} planes. These defects are so numerous that high resolution and further identification are impossible.

B. Discussion

There is little doubt that the etch pits correspond to points where dislocations emerge from the crystal. Furthermore, we can identify the etch lines as corresponding to stacking faults. However, we need to substantiate this. We first eliminate the other possibilities:

1. Dislocations. It would seem that the lines might simply be dislocations that are so close together that individual pits cannot be resolved. However, the evidence is against this interpretation. First, since no etch pits appeared on the {111}P face of the crystal in Fig. 4a, we conclude that aqua regia does not reveal dislocations on {111}P. Aqua regia does reveal lines; hence, the lines must not correspond to dislocations. Second, a large amount of plastic deformation would be expected to result in clusters of

- 5 -

dislocations, not single straight lines. We have seen clusters of etch pits as dense as $3x10^7$ cm^{-2}, and the pits did not lie in perfectly straight lines.

2. Simple twinning. This is impossible. A twin cannot end in the middle of a crystal; it must go all the way through the crystal. Figure 2 shows many lines which stop in the middle of the crystal.

3. Micro-twins (an even number of twins spaced only a few atom layers apart). There is no direct experimental evidence except electron microscopy that can rule out micro-twinning. Nevertheless, we eliminate this possibility because our experimental data is completely consistent with the model for stacking faults which is given below.

Stacking faults have been found and unambiguously identified in silicon epitaxial layers. We shall follow the treatment given by Booker and Stickler[2] in describing how stacking faults are formed.

When GaP grows in a {111}Ga direction, the various atomic layers may be labeled aa'bb'cc' aa'bb'cc'..., where the un-primed layers consist of phosphorus atoms, and the primed layers are gallium atoms. The layers in a perfect crystal are built up in a regular, repetitive sequence. Hornstra[4] has demonstrated that the layers always occur in pairs. Hence, it is sufficient to consider a stacking sequence abc abc ... We assume that vapor deposited layers are formed by the nucleation and two dimensional growth process. As a specific example, let the top layer of the seed be an "a" layer.

Then there are two ways the first epitaxial layer may form; it may be either a "b" or a "c" layer. If the overgrowth is perfect, the first layer will be a "b" layer. This will be followed by cabcabc ... . In this way a perfect zincblende lattice of GaP will be built up. Suppose, however, that the first layer of the overgrowth is not perfect. Let there be several nucleation points. Assume that most regions have nucleated as "b" layers but that one has nucleated as a "c" layer. When the first layer is completed, these regions have grown together, and the region of "c" layer is a stacking fault. This is the region shown inside the triangle in Fig. 8a. Now there are two ways the fault can continue to grow. That region has begun as "ac". It must resume growing in the usual sequence so that the zincblende lattice will be formed. It may do this either as acabcabc ... or as acbcabcabc ... . In the first case a layer (the "b" layer) has been left out and the defect is called an intrinsic stacking fault; in the second case there is an extra layer (the "c" layer) and the fault is extrinsic. A diagram of the second layer of an intrinsic stacking fault is shown in Fig. 8b. The defect has retained its shape, and it has grown slightly larger. Analysis shows that as succeeding layers grow, the defect will continue to retain its shape, and its boundaries will propagate up the {111} planes that are inclined to the growth plane. These boundaries are also stacking faults. Thus, the stacking faults grow upward through the crystal on {111} planes as in Fig. 8c.

There are several shapes that a set of stacking faults might take. The simplest form is the case we have been discussing.

The intersection of the inclined stacking faults with the growth surface always appears as an equilateral triangle. The triangle grows progressively bigger as the overgrowth gets thicker. This is diagrammed in Fig. 9a. The triangle may have one corner truncated. Then two parallel faults (one intrinsic and one extrinsic to minimize strain) grow upward through the crystal, each continually getting wider. These faults may be only 30-300 $\overset{\circ}{A}$ apart, so they would look like a single line in an etch pattern (Fig. 9b). If the triangle has two corners truncated, it quickly assumes the shape of a parallelo-gram, and then it propagates through the crystal with constant cross-sectional area (Fig. 9c). If all three corners of the triangle are truncated, the triangle shrinks and disappears as the layer grows (Fig. 9d). A shape like Fig. 9e would give an etch pattern that looked like a "V"

Stacking faults that intersect each other may interact. If both faults are intrinsic (or both extrinsic), the faults will annihilate each other as in Fig. 10. If one fault is intrinsic and the other is extrinsic, the cancellation will be incomplete as in Fig. 10b.

All of our experimental results are consistent with this model. In the first place, our etch patterns look exactly like those given by Chu and Gavaler[5]: the groove bottom is rough and one wall of the groove is steeper than the other. [However, just as etch pits point in $\langle\bar{2}11\rangle$ directions in Si and in $\langle2\bar{1}\bar{1}\rangle$ directions in GaP, the steep side of the groove is the $\langle2\bar{1}\bar{1}\rangle$ side in Si and the $\langle\bar{2}11\rangle$ side in GaP.] Moreover, the faults in GaP lie on the {111} planes

and they propagate through the crystal. As the model suggests, there are no stacking faults parallel to the growth plane that are large enough to be seen (see Fig. 5). Figure 2a is consistent with another feature: if the faults begin growing as sides of a tetrahedron, then no etch line can be longer than $\sqrt{\frac{3}{2}}$ times the distance from the substrate. Finally, the interactions shown in Fig. 6 may be explained in diagrams similar to Fig. 9. The fault that grows in length as the crystal gets thicker may do so as in Fig. 11a. The fault that gets shorter may do so as in Fig. 11b.

No clear cut model has been developed to explain how stacking faults are initiated. It seems likely that they can be started at a point where there is a damaged region in the substrate or at a point where there is an impurity (dust on the substrate, lapping grit on the substrate, etc.). There is little doubt that stacking faults are generally initiated at the substrate/overgrowth interface. This model for the initiation of stacking faults is, however, apparently not complete. It does not explain why there seem to be more stacking faults in $GaAs_xP_{1-x}$ alloys as the per cent of phosphorus is increased. We found on three typical samples that $GaAs_{.84}P_{.16}$* had 80 cm^{-1} stacking faults ($\frac{\text{total fault area}}{\text{volume}}$), $GaAs_{.7}P_{.3}$* had 350 cm^{-1}, and GaP had 700 cm^{-1}. The model also does not give any obvious reason why the etch lines usually have a predominant direction (see Fig. 2b) after the crystal is a few hundred microns thick. This direction is found experimentally to be

---

*$GaAs_xP_{1-x}$ was grown by A. Majerfeld in the same system that is used to grow GaP.

roughly parallel to the temperature gradient in the crystal growth furnace and to the gas flow direction in the furnace.

Diffusion of Zinc into GaP

A. Experimental

Elemental zinc was diffused into an undoped sample of GaP. The GaP sample had been lapped smooth with #3200 grit and measured 0.4 mm x 2.0 mm x 4.0 mm. It and 0.1 mg of zinc were placed inside a 3 mm inside diameter x 11 mm quartz tube. The tube was evacuated to 1×10^{-3} mm Hg and was sealed. The ampoule was then heated to 1000°C for 15 minutes. At the end of that time the ampoule was quenched and broken open. The {111}Ga face of the sample was angle lapped at an angle of 5° and the beveled face was polished in 0.3 μ grit. Finally, the sample was etched in the {111}Ga solution to reveal both the diffusion front and the imperfections. Photomicrographs of the resulting etch patterns appear in Fig. 12.

Several features appear in this figure. The irregularity of the diffusion front is striking. The angle of the bevel makes every 100 μ along the crystal surface in a direction perpendicular to the diffusion front correspond to a 10 μ change in depth. Thus the diffusion spike shown in the high magnification photograph of Fig. 12 has penetrated 3.5 μ farther into the crystal than has the rest of the diffusion front in the immediate vicinity. On the other hand, the "island" in the p region in the same figure corresponds to diffusion that is 3.5 μ shallower than in the surrounding region. It is clear from the photomicrographs that deeper penetration takes place in regions where there are etch pits (dislocations) and

lines (stacking faults). We also see that there is a double

diffusion front. The shallow front separates a region of very dense

etch pits from a region of a more normal density of etch pits. The

deeper front separates two regions which have different etching rates.

This double front is similar to the one seen by Black and Jungbluth[6]

in GaAs. They find that the shallower junction separates p^+ and p

regions, and the deeper junction separates p and n.

B. Discussion

Increased diffusion rates through dislocated regions

in crystals are expected. Increased diffusion rates down stacking

faults are not unexpected according to Abrahams and Buiocchi[7] since

the faulted region is effectively a different kind of crystal structure

from the rest of the lattice. However, Williams[8] specifically found

that zinc does not exhibit an increased diffusion rate at stacking

faults in $GaAs_xP_{1-x}$. Of course, many more experiments need to be

carried out before we can draw any conclusions about the mechanism of

zinc diffusion near imperfections in GaP. We may expect, however,

to find that the diffusion conditions - temperature, phosphorus

overpressure, doping of the host crystal - will have a significant

effect on the depth and planarity of diffusion. In particular, our

vapor deposited GaP crystals are grown at $820^{\circ}C$ and are then slowly

cooled to room temperature. Thus the vacancy concentration in a

crystal would be in equilibrium at some temperature below $820^{\circ}C$.

When we diffused at $1000^{\circ}C$, the crystal was not in equilibrium in

two senses: the zinc was diffusing in, and the vacancy concentration

was not in equilibrium. It is conceivable that we might have gotten

- 11 -

different results if we had prepared the crystal before diffusion in such a way that the vacancy concentration would have been in equilibrium at 1000°C. In fact, it is not inconceivable that stacking faults would act as diffusion short circuits under one set of diffusion conditions and not another. These are things that will have to be learned through further experimentation.

The heavy etch pitting in the region between the surface and the first diffusion front may be due to precipitation of zinc. We have observed that regions diffused with zinc become opaque. Furthermore, Black and Jungbluth[6] have demonstrated that zinc precipitates in the region between the surface and the first diffusion front in GaAs. These characteristics of zinc diffusion in GaP will, of course, also have to be determined by further experimentation.

REFERENCES

1. S. F. Nygren, Quarterly Progress Report, Stanford University, for period April 1 - June 30, 1966.

2. G. R. Booker and R. Stickler, J. Appl. Phys., 33, 3281 (1962).

3. Edward L. MacKenna, Stanford University, DMS Master's Report #66-5 (1966).

4. J. Hornstra, J. Phys. Chem. Solids, 5, 129 (1958).

5. T. L. Chu and J. R. Gavaler, J. Electrochem. Soc., 110, 388 (1963).

6. J. F. Black and E. D. Jungbluth, J. Electrochem. Soc., 114, 181 (1967).

7. M. S. Abrahams and C. J. Buiocchi, J. Appl. Phys., 36, 2855 (1965).
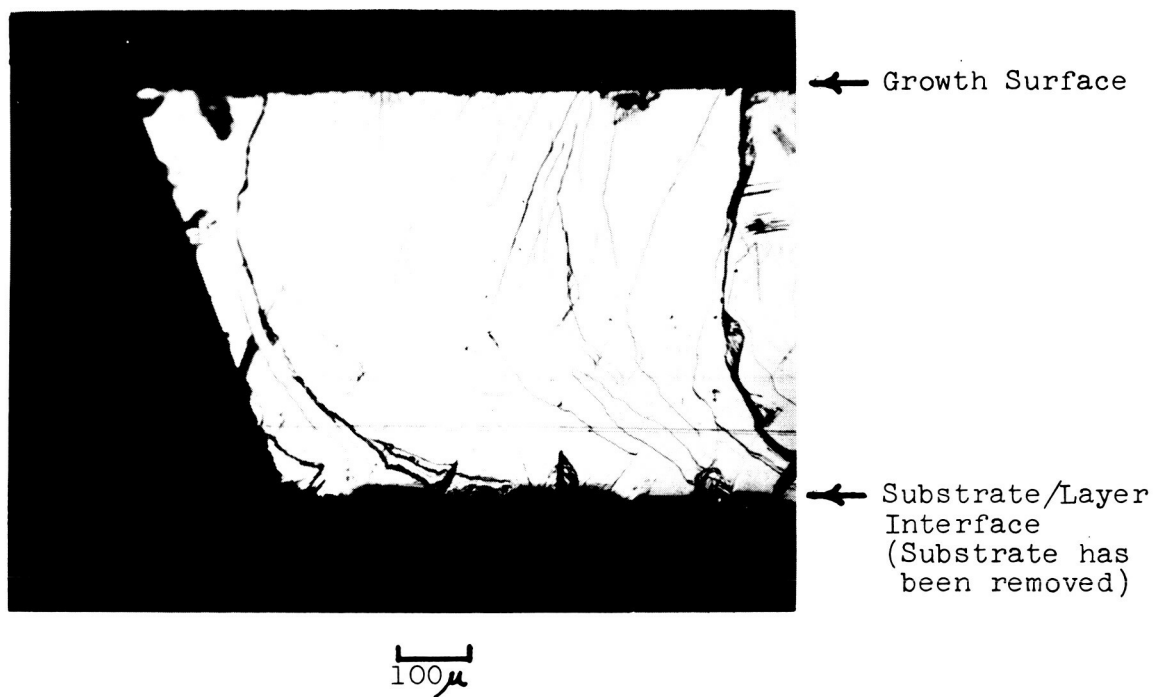
8. Forrest V. Williams, private communication.

← Growth Surface

← Substrate/Layer
Interface
(Substrate has
been removed)

100μ

Figure 1: Etch Figure on {110} surface of GaP.
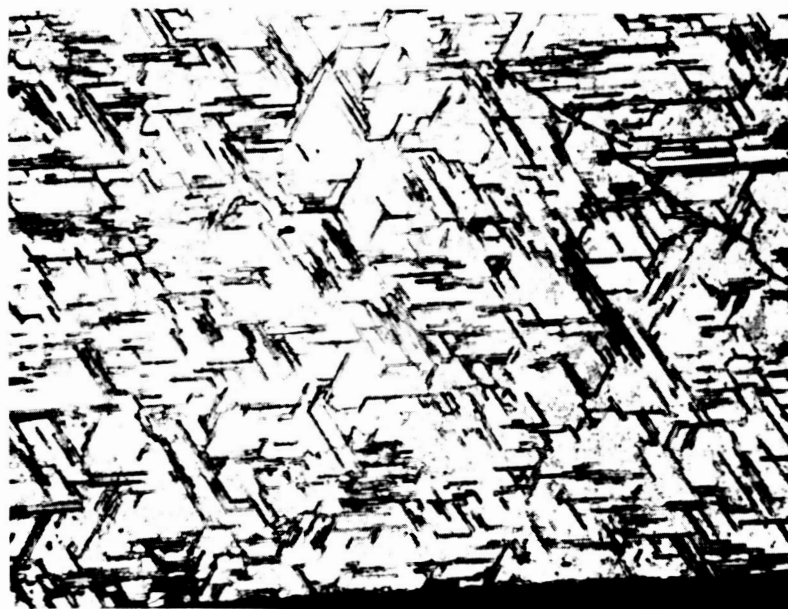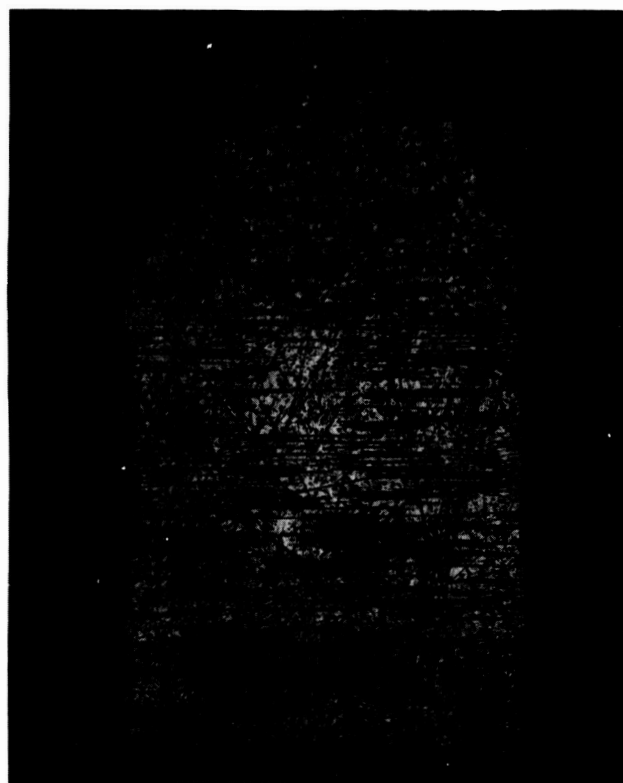   (Cleavage face etched in 9 HNO_3 : 1 HF : 5 H_2O)

Figure 2a: Etch Figure on $\{111\}$ Ga surface of GaP about 70μ from substrate/layer interface.

Figure 2b: Etch Figure on $\{111\}$ Ga surface of GaP about 400μ from substrate/layer interface. (Polished surface etched in 8g $K_3Fe(CN)_6$: 12g KOH : 100g H_2O)
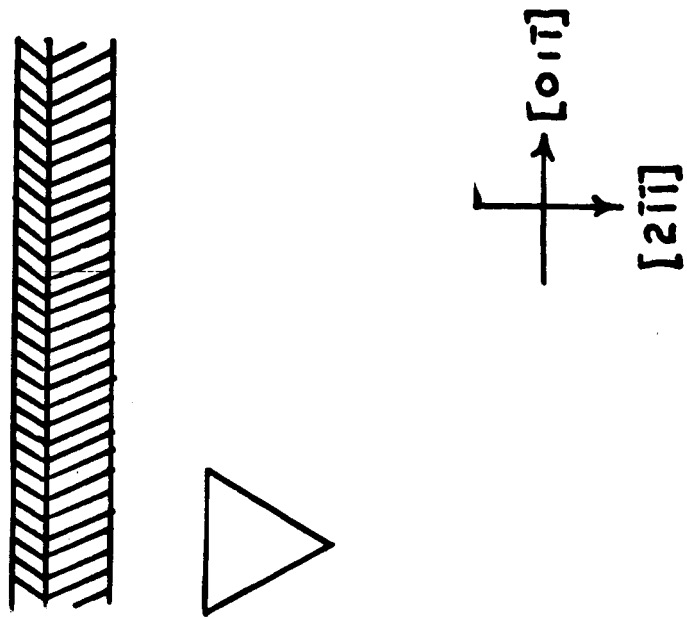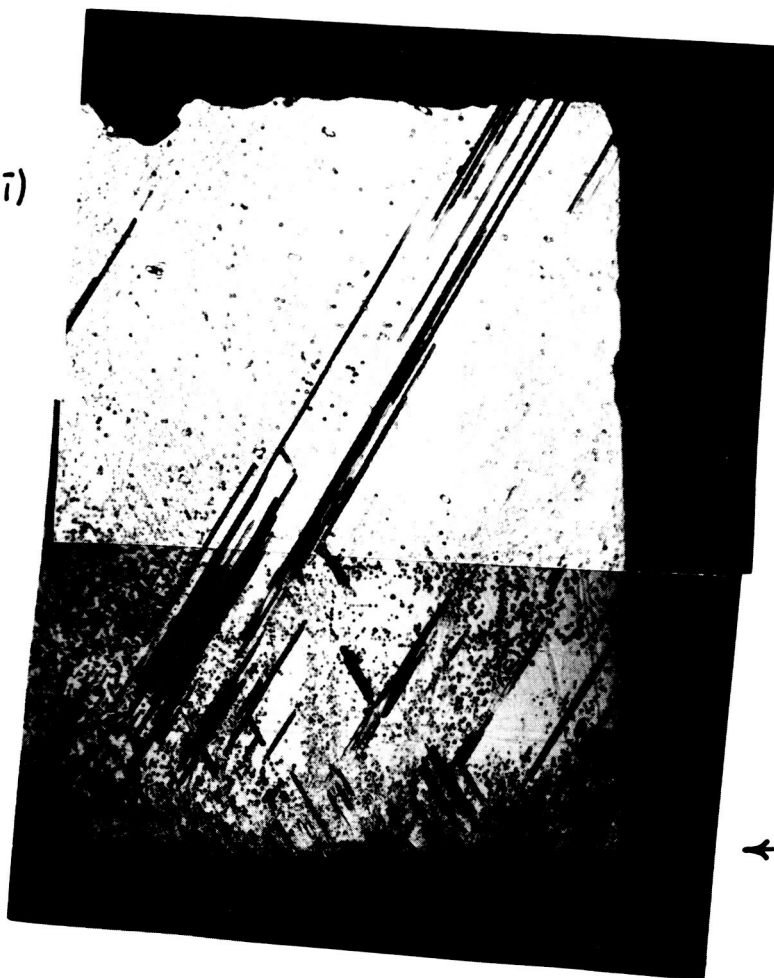
Figure 3: Schematic diagram of etch figures on (111) surface

100μ
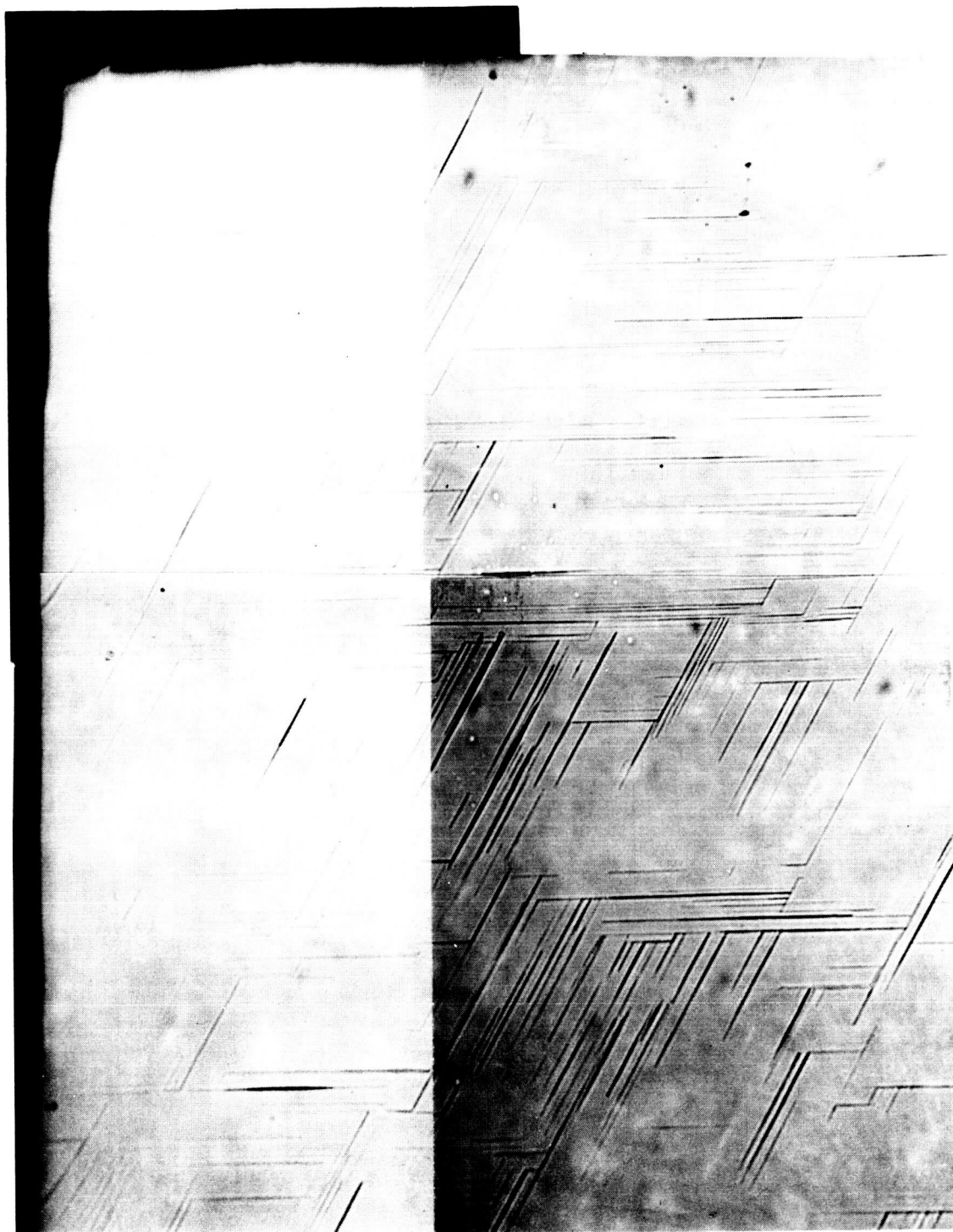
Figure 4a: Etch figure on {111} P surface of GaP.
(Polished surface etched in hot aqua regia)
The {111} Ga surface of this sample is shown in Figure 4b.

|——————|
100µ

Figure 4b: Etch figure on {111} Ga surface of GaP.
            (Polished surface etched in hot aqua regia)
            The {111} P surface of this sample is shown in figure 4a.
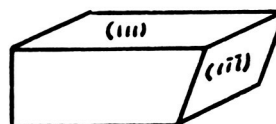
(111)

(1$\bar{1}\bar{1}$)

Figure 5: Etch
Figures on (111)
Growth Surface and
(1$\bar{1}\bar{1}$) Cross Section.

(Polished surfaces
etched in {111} Ga
solution)

← Growth Surface

(111)

(1$\bar{1}\bar{1}$)

├─ 100μ ─┤

←Substrate/Layer
Interface

$[2\bar{1}\bar{1}]$

$[0\bar{1}\bar{1}]$

(III) PLANE

213μ from substrate

248μ from substrate

300μ from substrate

370μ from substrate
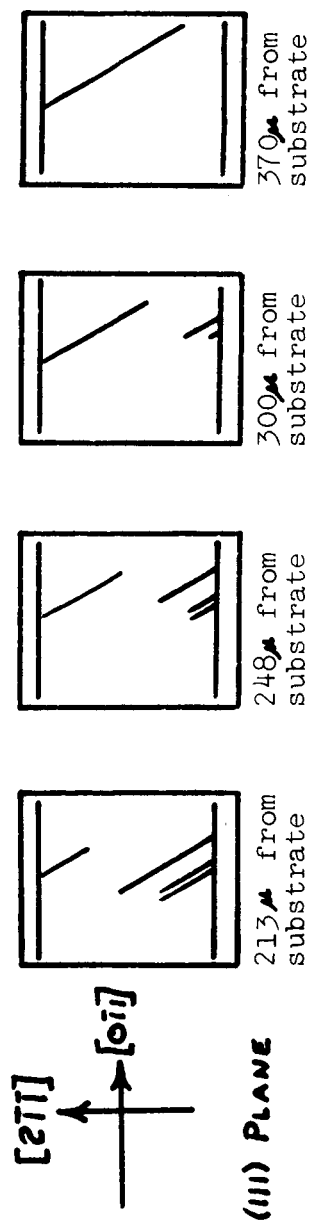
Figure 6: Schematic diagram of interactions among etch figures.

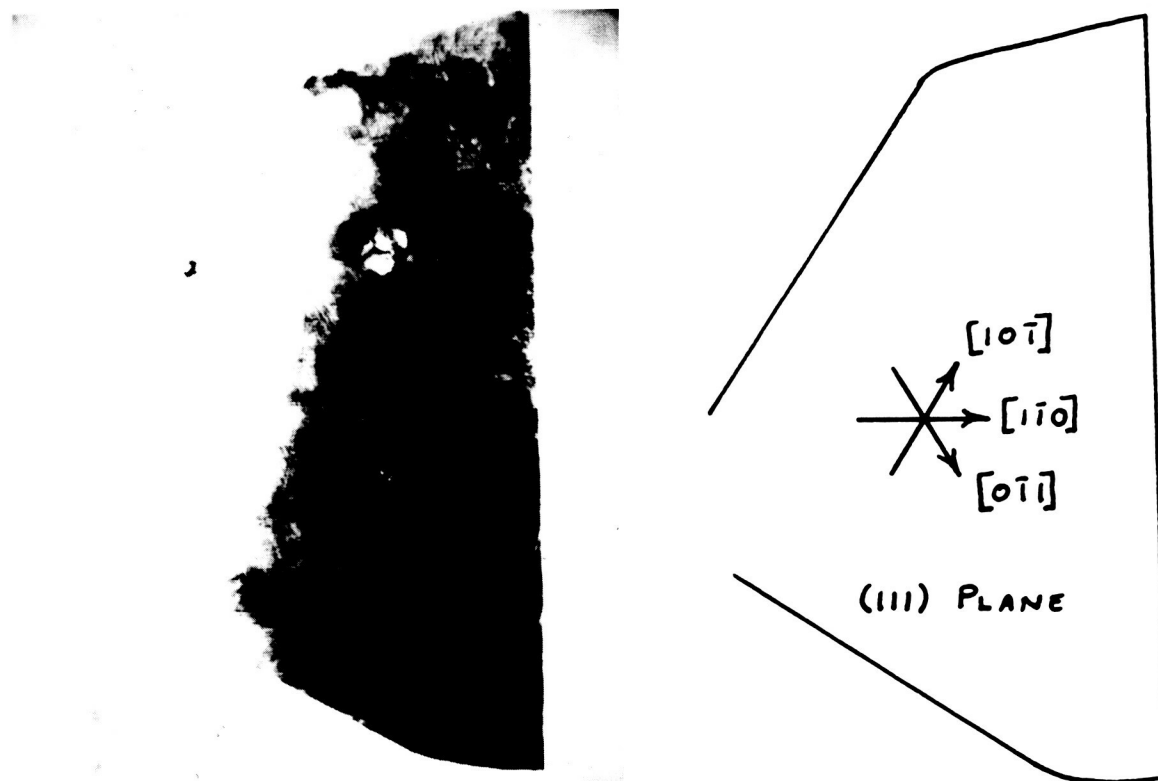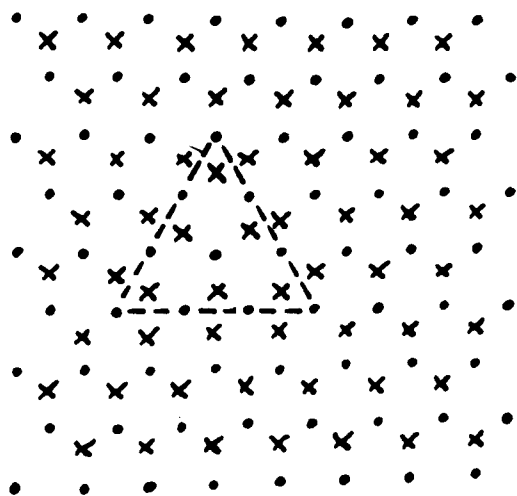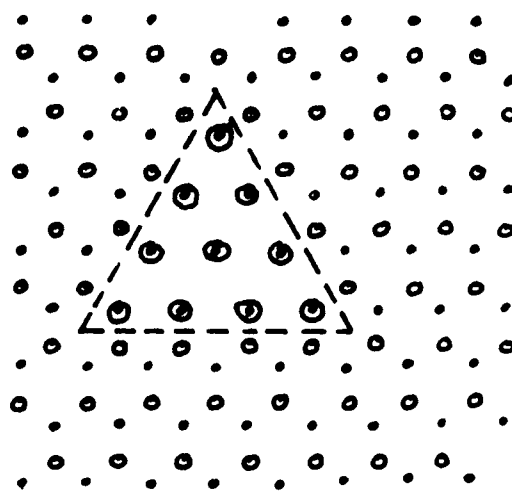[10$\bar{1}$]

[1$\bar{1}$0]

[0$\bar{1}\bar{1}$]

(111) PLANE

Figure 7: Berg-Barrett x-ray topograph of GaP crystal.
(044) reflection.
Magnification is about 20X.

Atom Layer n=0, Substrate
● Layer, Type "a" Positions

Atom Layer n=1, Epitaxial
✗ Layer, Outside △ - Type "b"
          Inside △ - Type "c"

Figure 8a: Completion of first
layer of intrinsic stacking fault

Atom Layer n=0, Substrate
● Layer, Type "a" Positions

Atom Layer n=2, Epitaxial
O Layer, Outside △ - Type "c"
          Inside △ - Type "a"

Figure 8b: Completion of second
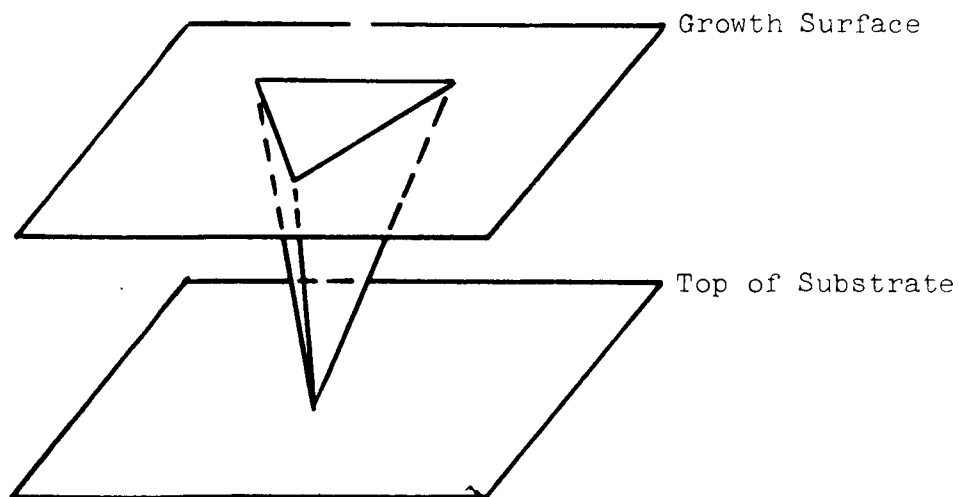layer of intrinsic stacking fault

Growth Surface

Top of Substrate

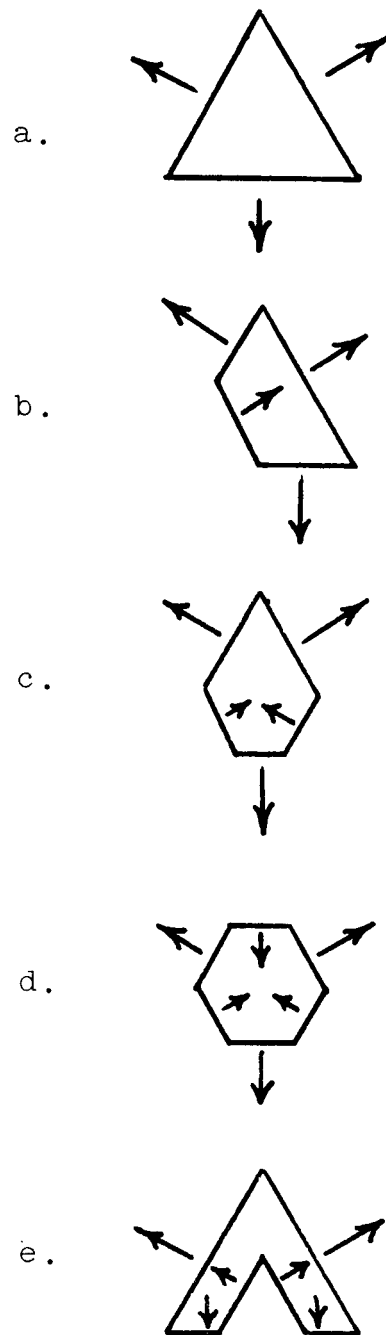Figure 8c: Stacking faults on inclined {111} planes.

Figure 9: Growth of various stacking fault configurations.

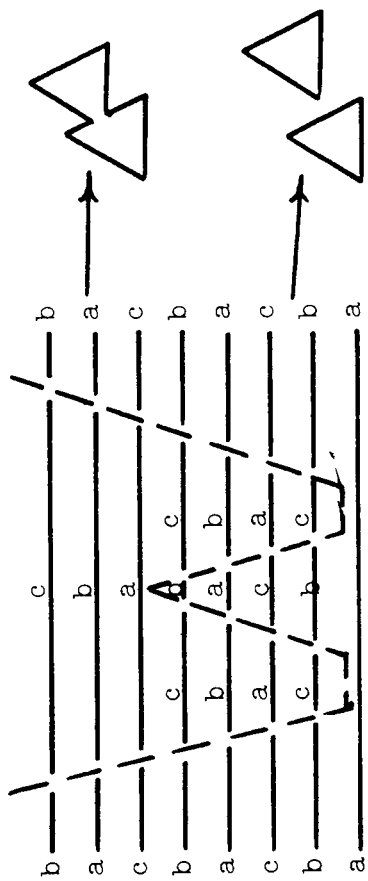Figure 10a: Interaction of two intrinsic stacking faults.
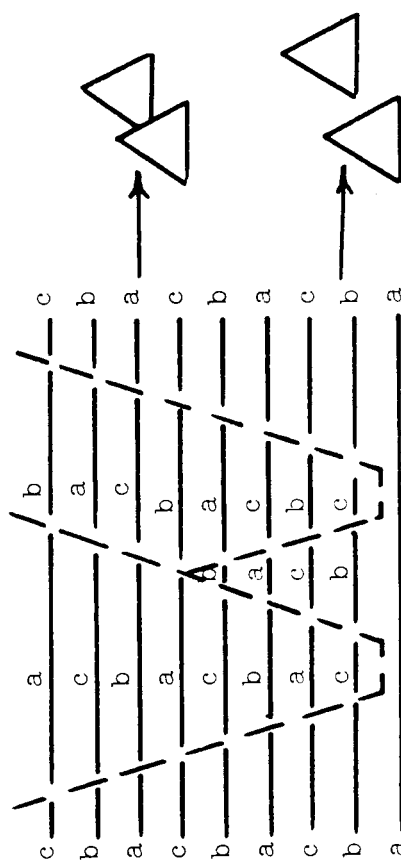
Figure 10b: Interaction of an intrinsic and an extrinsic stacking fault.

[2$\bar{1}\bar{1}$]
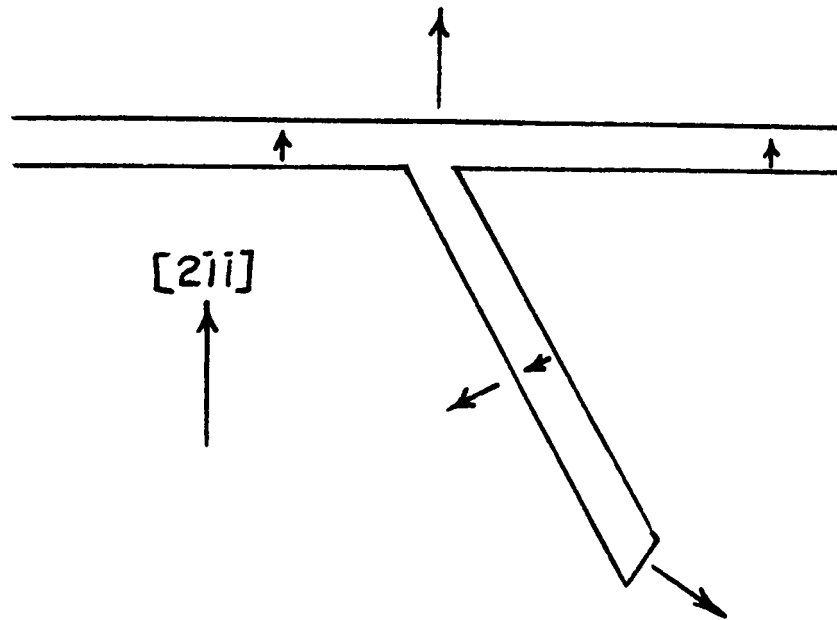
Figure 11a: Interactions among stacking faults.

[2$\bar{1}\bar{1}$]
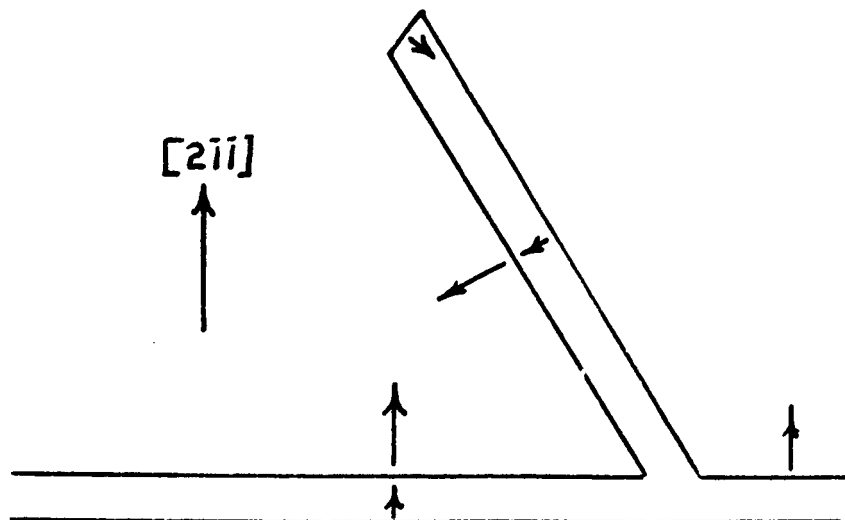
Figure 11b: Interactions among stacking faults.

P N

50μ

└─ Second Diffusion Front

P N

100μ

└─ Second Diffusion Front
└─ First Diffusion Front

Figure 12: Zinc diffusion
front in GaP. (Sample was
angle lapped, polished, and
etched in the {111} Ga solution.)

PROJECT 5116:   DONOR IMPURITIES IN GaP

National Aeronautics and Space Administration
Grant NsG-555
Principal Investigator: G. L. Pearson
Staff: A. Young*

The purpose of this project is to study the behavior

of shallow donors in gallium phosphide. In particular S, Se and Te

will be diffused into GaP to determine solubilities and diffusion

parameters. This information will be useful in delineating the

properties of GaP doped with these shallow donor impurities.

Radioactive Diffusions

High specific activity (1 mc/mg) sulfur-35 has been

received this quarter. The radio purity of this material is specified

to be 99^+%. Chemical purity, although unknown, is believed to be of

the same order of magnitude. After dilution with non-radioactive

sulfur (5 9's purity) and preparation of a calibration standard, a

number of diffusions were performed at temperatures between 1100 and

1200°C in the presence of phosphorus vapor. The experimental procedures

have been described in a previous report.[1]

The diffusion profiles and important parameters of two

radiotracer diffusions done this quarter are given in Figs. 1 and 2

and in Table I. The results obtained for the diffusion constant and

solubility of sulfur in GaP are summarized in Table II. These results

were obtained by a least-square fit of the complementary error function

to the experimental points.

---

*NSF Fellow

Experimental Results (Diffusion)

Several experimental difficulties were discussed in the last "Quarterly Progress Report". One was the error introduced by "wedging" during the lapping of the samples after diffusion; that is, lapping that was not parallel to the diffusion front. By suitable choice of the material used for the rubber pad in mounting the samples to the aluminum lapping button, this error has been minimized so that it is no longer a major problem.

Surface Deterioration

Much more serious is the surface deterioration of the sample. Even in the presence of phosphorus vapor, when sulfur is present, there is an appreciable weight loss of the sample during diffusion. The surface attack appears to be more severe on the "A" (gallium) face. Diffusion profiles are generally measured only on the "B" (phosphorus) face.

The amount of weight loss is not always the best indication of surface deterioration, since there can often be local redistribution of the sample without much weight loss. A better criterion is direct observation of the surface under low power magnification. Since the surfaces are polished with Linde A before diffusion, it is quite easy to see surface irregularities after diffusion.

Since we have not yet succeeded in keeping surface deterioration down to the point where it can be neglected completely, care must be taken in interpreting the diffusion profiles. The results shown in Table II are for a simple fit of the profile with

the solution for a constant source diffusion into a semi-infinite
sample:

$$N = N_s \ \text{erfc} \ (x/2\sqrt{Dt}).$$

Evaporating Surface

Alternatively, an upper bound for the diffusion
coefficient can be obtained from the solution for a surface evaporating
at a constant velocity v: [2]

$$N = \frac{1}{2} \ N_s \ [\text{erfc} \ \frac{x + vt}{2\sqrt{Dt}} + \exp \ \frac{-vx}{D} \ \text{erfc} \ \frac{x - vt}{2\sqrt{Dt}}].$$

The major error in this process is the determination of the velocity
v. If it is assumed that all the loss occurs on one face, the
diffusion constant is found to be several orders of magnitude larger.
However, it is known that surface deterioration is not equal on both
sides; if it is assumed that only one third of the total loss occurs
on the lapped side (loss on the "bad" side is twice that on the "good
side"), a more reasonable assumption, the diffusion constant is about
3-4 times larger.

Constancy of Vapor Source

Additional error is present because the sulfur vapor
pressure is not constant during diffusion. In the last quarterly
progress report it was noted that the sulfur pressure in diffusions
R-2 and R-3 changed by a factor of 2 or more during diffusion. A more
accurate calculation shows that practically all of the sulfur placed
in the ampoule was diffused into the sample.

Since we are using the sulfur and phosphorus pressures as the diffusion parameters (recall that at a fixed temperature in a solidus region of a ternary system there are 2 degrees of freedom) it is necessary that these be kept constant during the diffusion. In diffusions AL-1 and AL-4-A, the sulfur pressure changed by 20% and 10% respectively (lower limit only). The major differences between the diffusions done last quarter and those done this quarter are the larger amounts of sulfur, smaller samples, and shorter diffusion times - all of which help to keep the amount of sulfur in the sample small compared with the original amount in the ampoule.

Attempts to decrease the sulfur pressure by increasing the size of the ampoule while keeping the total amount of sulfur fixed failed. Over 1/3 of the sample was transported to the ampoule walls ($T = 1200^{\circ}C$, $t = 12$ hrs).

Compound Source

In order to maintain a constant but low sulfur pressure while retaining good surfaces, it may be necessary to use a sulfur compound such as Al_2S_3 for a source.[3] The sulfur pressure for a given compound is fixed by the temperature, but the pressure may be varied by using other compounds. Effect of the other component of the sulfur compound must be considered. Variation of solubility, etc. may still be effected by varying the phosphorus pressure.

Quartz Flats

It has been reported that good surfaces have been maintained during the diffusion of selenium and tin into GaAs by

sandwiching the sample between quartz plates.[4,5] This is a useful

technique in device fabrication. However, the diffusion conditions

become somewhat unclear since the close spacing between the quartz

plate and sample may present a barrier to the diffusant.

Phosphorus was diffused into p-type silicon to form a

p-n junction. During diffusion, the silicon wafer lay flat on a

quartz platform. It was of some interest to compare the diffusion

on both sides of the wafer to see if the presence of the platform did,

in fact, inhibit diffusion from the bottom side.

Sheet resistivity and junction depth measurements were

made on the two sides as shown in Table III. The results indicate

a higher sheet resistivity and shallower junction depth from the

bottom side. This is what would be expected if the kinetics for

diffusion were not as favorable because of the close spacing between

wafer and platform.

Additional information could be obtained by making

incremental sheet resistivity measurements of the diffused layer.

At this time, no results are available.

Checks on Radiotracer Profile

It is always desirable when doing radiotracer diffusions

to have an independent check on the results. Such checks include auto-

radiographic studies to ensure that the impurity radiation emanates

uniformly from the sample and not from a few localized hot spots, p-n

junction depth measurements, and electrical measurements on the

diffused layer.

During the last quarter autoradiographs were taken at the surfaces of the samples as diffused, and occasionally at a point beneath the surface. No gross inhomogenities were seen. However, a more careful study is necessary.

Autoradiographs were taken with Kodak Projector Slide Plates. Good exposures were obtained with 30-minute exposures for activities of 1.5×10^6 counts per minute per square centimeter. Counting efficiency for our proportional counter and sulfur-35 is 5%.

Attempts were made to measure the free carrier concentration of the diffused layer by means of a plasma minimum technique which has been quite successful in InAs.[6] No distinct minimum was observed. It has been reported that this technique is more difficult in low mobility, high loss materials such as GaP and p-type GaAs.[7]

Annealing Experiments

Several GaP samples were annealed (without sulfur) at 1100°C, both in the presence and absence of phosphorus. The purpose of these experiments was to see if any significant changes in impurity concentration or mobility occurred after annealing in the absence of any intentionally added impurity.

Some care was taken to exclude copper. The quartz ampoules were soaked in aqua regia and then a 10% KCN solution for several hours, rinsed in deionized water and then methanol. The GaP samples were soaked in a warm KCN solution for several hours and then rinsed. They were then transferred to the ampoules with a piece of filter paper.

The samples were annealed at 1100°C for 12 hours.
Measurements of the electrical properties of these samples before
and after annealing are shown in Table IV. As expected the sample
annealed in the presence of phosphorus retained a better surface.
(The error in the measurement of the sample annealed in phosphorus is
quite large due to poor contact placement so no special significance
should be given to the high hole mobility.)

The samples before anneal were n-type. Ohmic contacts
were made with tin. After the anneal, ohmic contacts were obtained,
not with tin, but with an Au-2% Zn alloy (indium contacts were also
successful) indicating that the material had been converted to p-type.
This conclusion was confirmed by the sign of the Hall voltage. Such
thermal conversion has been observed in Ge[8] and GaAs[9] and is generally
attributed to copper contamination - residual copper not removed by
the KCN treatment, copper within the quartz ampoule, in the phosphorus,
or even in the rinse water or methanol.

Since the original crystal had an electron concentration
of 10^{16} cm^{-3}, the total copper contamination in these experiments is
at least of this order. For diffused layers with high carrier
concentration, thermal conversion may not be a serious problem.
However, if Cu has a deep level, the total concentration may be much
greater than 10^{16}.[10]

REFERENCES

1. A. Young, Quarterly Progress Report, Stanford University, September 30 - December 30, 1966.

2. T. I, Kucher, Soviet Physics-Solid State, $\underline{3}$, 401 (1961)

3. R. G. Frieser, Spring Meeting of Electrochem. Soc., Toronto, 1964 (author with Bell Telephone Laboratories).

4. W. Von Munch, IBM J. Res. and Devel., $\underline{10}$, 438 (1966).

5. R. W. Fane and A. J. Goss, Solid State Electronics, 6, 383 (1963).

6. D. Edwards and P. Maker, J. Appl. Phys., $\underline{33}$, 2466 (1962).

7. L. A. Murray, J. J. Rivera, P. A. Hoss, J. Appl. Phys., $\underline{37}$, 4743 (1966).

8. B. I. Boltaks, Diffusion in Semiconductors, Academic Press New York, 1963, p. 167.

9. O. Madelung, Physics of III-V Compounds, J. Wiley and Sons, Inc., New York, 1964, p. 253.

10. J. W. Allen and R. J. Cherry, SERL Tech. Jour., $\underline{13}$, 57 (1962).

FIGURE CAPTIONS

Fig. 1   Diffusion Profile of Sulfur in GaP (Diffusion AL-1)

Fig. 2   Diffusion Profile of Sulfur in GaP (Diffusion AL-4-A)

Diffusion	AL-1	AL-4-A
Diffusion Temp.	$1216^{O}C$	$1122^{O}C$
Diffusion Time	12 hrs.	12 hrs.
Ampoule Volumn	1.39 ml.	4.3 ml.
Wt. GaP (before diffusion)	49.641 mg.	30.826 mg.
Wt. GaP (after diffusion)	47.629 mg.	29.832 mg.
Wt. loss	2.012 mg.	0.994 mg
% Wt. Loss	4%	3.2%
Equiv. Surface Loss	12 μ	6.5 μ
Wt. Sulfur	63.7 μg	63.7 μg
Sulfur Density	45.7 μg/ml.	14.7 μg/ml.
S_2 Pressure	8.8×10^{-2} atm.	2.5×10^{-2} atm.
Wt. Phosphorus	1.754 mg.	4.850 mg.
Phosphorus Density	1.26 mg/ml.	1.13 mg/ml.
P_2 Pressure	0.84 atm.	0.7 atm.
P_4 Pressure	0.80 atm.	0.4 atm.
Sample Thickness	12 mils	8 mils
Vacuum	5×10^{-4} torr.	3×10^{-3} torr.

TABLE I

Diffusion Parameters

| Diffusion	Temperature	$D(cm^2/sec)$	$Ns(cm^{-3})$
AL-1	$1216^{\circ}C$	1.9×10^{-12}	7.3×10^{20}
AL-4	$1122^{\circ}C$	1.0×10^{-12}	8.0×10^{20}

TABLE II

Diffusion Constant (D) and Surface Concentration (Ns)
of Sulfur in Gallium Phosphide*

*Diffusion Conditions given in Table I.

Side	Sheet Resistivity $p_s (\Omega/\square)$	Junction Depth x_j (mils)
UP	1.38	1.03 ± 0.12
DOWN	2.53	0.91 ± 0.12

TABLE III

Comparison of Diffusion Parameters for Silicon Wafer on
Quartz Platform (Phosphorus Diffusion)
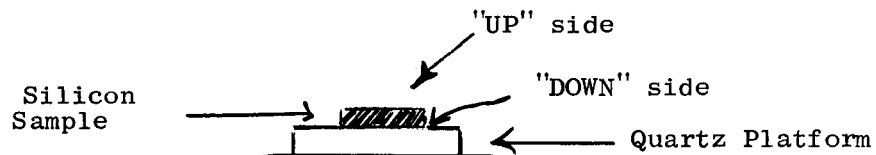
12 hrs @ $1100^{\circ}C$ vacuum 5 microns

	Before Anneal Crystal DR-1	After Anneal with phosphorus	After Anneal (no phosphorus)
Type material	N	P	P
Hall Mobility μH (cm^2/v-sec)	97	120	41
Carrier Conc. (cm^{-3})	$n=10^{16}$	$p \approx 4.6 \times 10^{14}$	$p=1.6 \times 10^{14}$
Resistivity ρ (ohm-cm)	6	112	970

TABLE IV

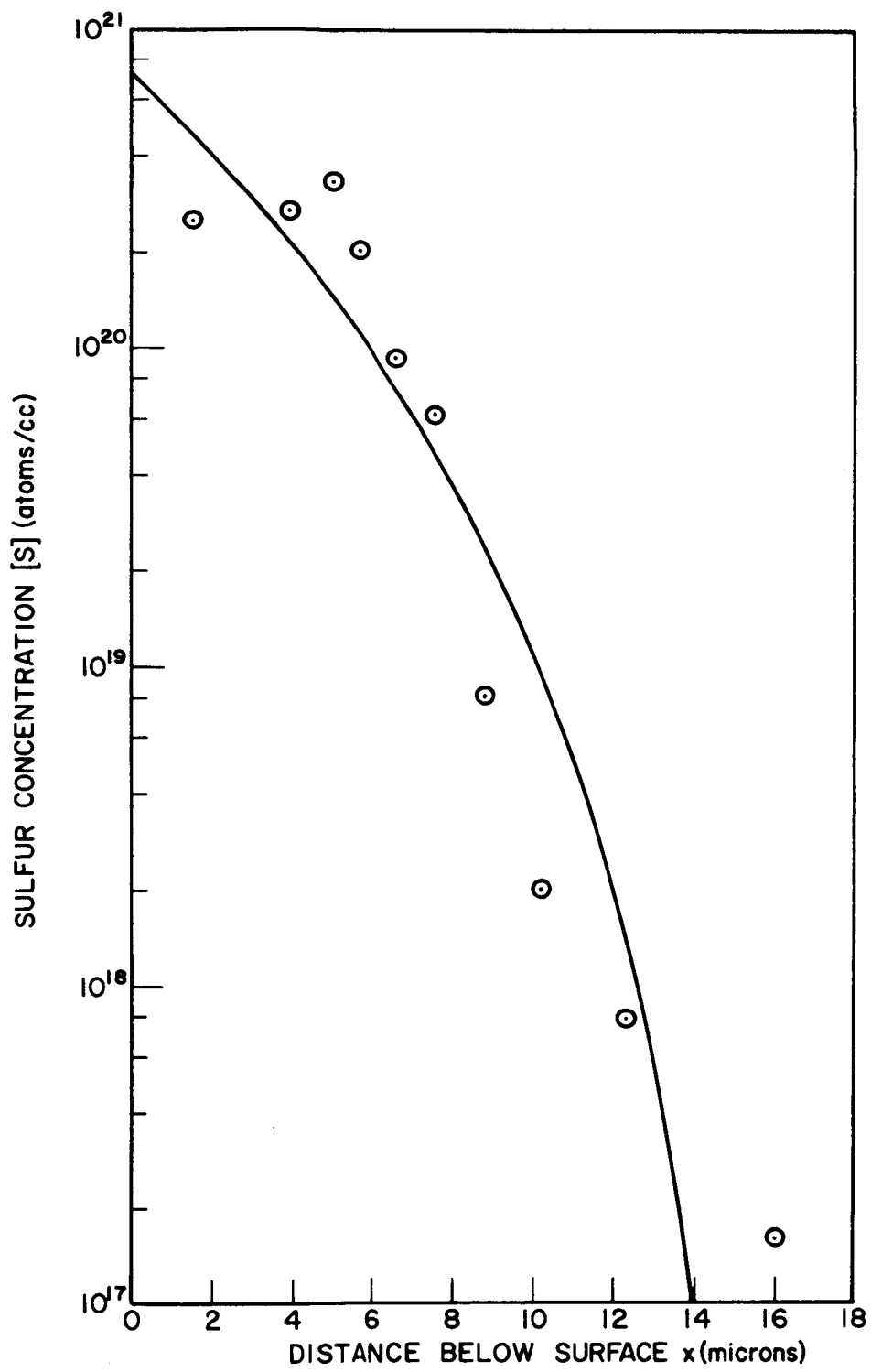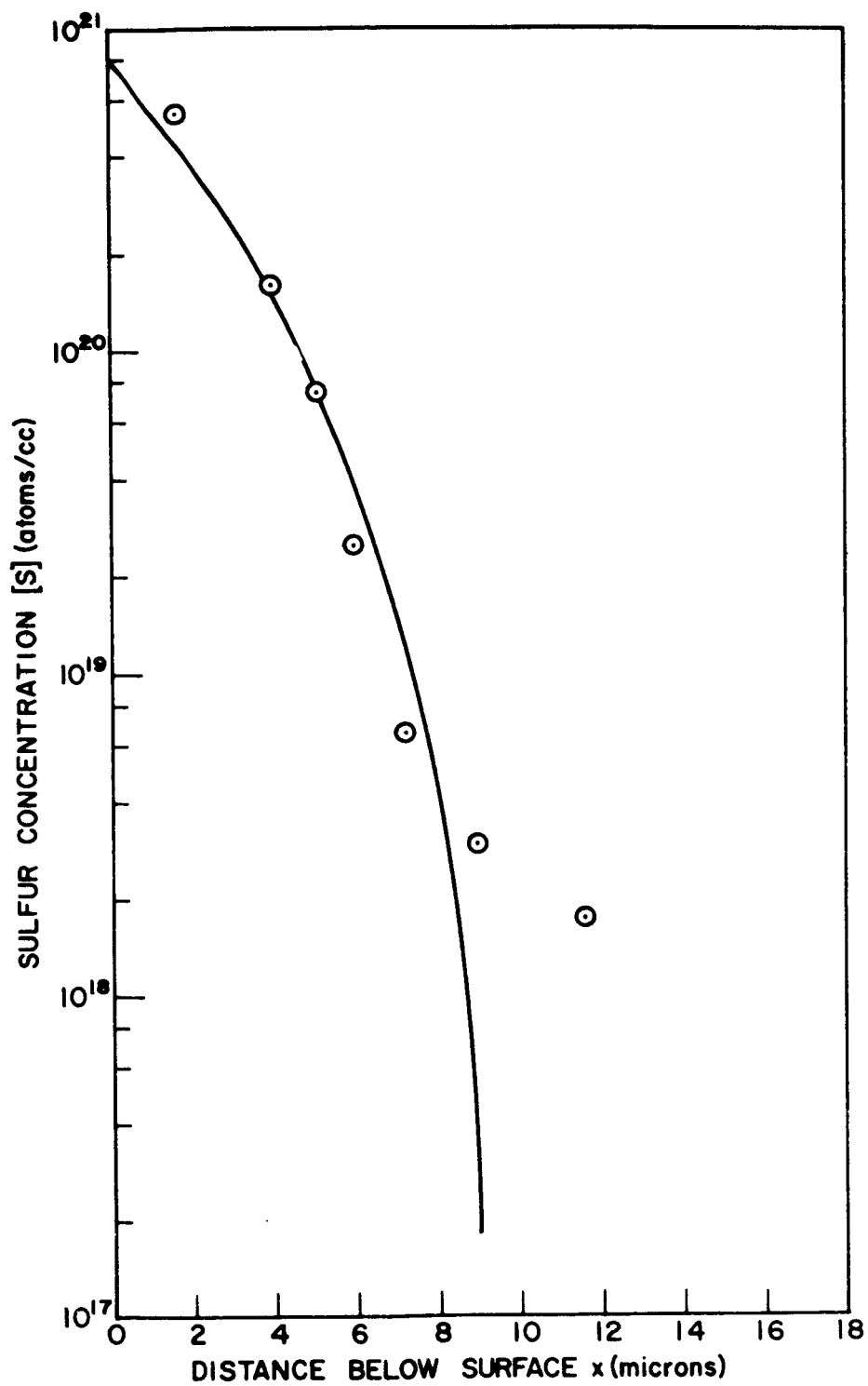Effect of Annealing on Electrical Properties of Undoped GaP

Fig. 1

Fig. 2